Mechanical strength of wet particle agglomerates

Thanh-Trung Vo, Patrick Mutabaruka, Saeid Nezamabadi, Jean-Yves Delenne, Edouard Izard, Roland Pellenq, Farhang Radjai

Mechanical strength of wet particle agglomerates

Thanh-Trung Vo[a, b], Patrick Mutabaruka[c], Saeid Nezamabadi[a], Jean-Yves Delenne[d], Edouard Izard[e], Roland Pellenq[c], Farhang Radjai[a, c, *]

[a] LMGC, Université de Montpellier, CNRS, Montpellier, France
[b] Bridge and Road Department, Danang Architecture University, Da Nang 553000, Vietnam
[c] ⟨MSE⟩², UMI 3466 CNRS-MIT, MIT Energy Initiative, 77 Massachusetts Avenue, Cambridge 02139, United States
[d] IATE, UMR1208 INRA - CIRAD - Université de Montpellier SupAgro, 34060 Montpellier, France
[e] ArcelorMittal R&D Maiziéres, Voie Romaine, F-57283, Maiziéres-Ls-Metz, France

Using particle dynamics simulations, we investigate the strength and microstructure of agglomerates of wet frictional particles subjected to axial compression. The numerical model accounts for the cohesive and viscous effects of the binding liquid up to a debonding distance with the liquid assumed to be dis- tributed homogeneously inside the agglomerate. We show that wet agglomerates undergo plastic defor- mation due to the rearrangements of primary particles during compression. The compressive strength is thus characterized by the plastic threshold before the onset of failure by the irreversible loss of wet contacts between primary particles. We find that the agglomerate plastic threshold is proportional to the characteristic cohesive stress defined from the liquid-vapor surface tension and the mean diameter of pri- mary particles, with a prefactor that is a nearly linear function of the debonding distance and increases with size span. We analyze the agglomerate microstructure and, considering only the cohesive capillary forces at all bonds between primary particles, we propose an expression of the plastic strength as a func- tion of the texture parameters such as the wet coordination number and packing fraction. This expression is shown to be consistent with our simulations up to a multiplicative factor reflecting the distribution of the capillary bridges.

Keywords:
Granular matter Agglomerate, Capillary force law Discrete element method Plastic strength Diametrical compression

1. Introduction

The agglomeration or granulation of solid particles is used in many sectors including powder metallurgy, chemical engineering, pharmaceutical industry, and iron-making processes to produce agglomerates or granules from small particles. The agglomerates are used to improve flow properties, enhance permeability for the interstitial gas or reduce segregation in the presence of several types of particles [1–4]. The binding material is generally a liquid, which is mixed with the primary particles in a granulator [5–8]. Hence, the mechanical strength of the 'raw granules' produced by the agglomeration of primary particles is ensured by the action of capillary and viscous forces due to the presence of liquid clusters in the pore space [9–14].

The raw granules should be in a densely and homogeneously packed state in order to support the loads to which they are subjected during subsequent operations and give rise to strong solid granules upon sintering [15–19]. The granule strength is controlled by two types of parameters: 1) process parameters such as the method of mixing particles with the liquid (depending on the granulator) [20,21] and 2) material parameters such as the nature of the liquid and the size distribution of the particles [6,21,22]. The physical processes governing the growth of granules are complex due to the dynamic nature of granulation involving the collisions of particles and transport of the binding liquid inside a partially wet granular material [9,23–27]. The agglomeration process in a fluidized bed can be correctly modeled by assuming binary collisions between wet particles [7,8,28] whereas in a rotating drum [29], for example, the agglomeration occurs inside a dense cohesive granular flow whose rheology has only recently been studied by careful experiments [30–33] and simulations [20,34].

The effect of material parameters on the granule strength reflects both the strength of cohesive bonds between particles and the granular texture, i.e. the organization of the primary particles inside the granule. For example, the strength of pharmaceutical tablets, measured by quasi-static compression between two platens, declines with porosity, which is a function of the consolidation pressure used to manufacture the tablet [35,36]. In the same way, the compressive strength of cohesive powder mixtures

* Corresponding author.
E-mail address: franck.radjai@umontpellier.fr (F. Radjai).

is an increasing function of the relative density [37]. The diametrical compression test is a simple way of measuring the tensile strength of powder compacts as the compressive strength (the stress at incipient failure of a granule) is proportional to the tensile strength of the granule [38]. This method has, however, been mostly used to study the fracture stress of brittle materials composed of particles glued via solid bonds [39–41]. In contrast, wet granules have been much less investigated. While their cohesive strength is mainly controlled by the Laplace pressure and surface energy of the liquid phase, the effects of granular texture resulting from the granulation process and material parameters are still poorly understood.

In this paper, we are interested in the influence of material parameters on the strength of wet spherical agglomerates in which the liquid is assumed to be distributed as binary bridges joining eligible particle pairs. We use the Discrete Element Method (DEM) with a capillary cohesion law in which the attraction force is an explicit function of the gap between particles and liquid-vapor surface tension, and the amount of liquid is mainly accounted for by a debonding distance. By simulating the diametrical compression of spherical agglomerates, we find that, due to particle rearrangements, they show a plastic behavior with a threshold that we analyze as a function of friction coefficient and size span of primary particles. We also introduce a model for the compressive granule strength that accounts for particle size distribution and we discuss the role of the class of fine particles for the plastic threshold.

In Section 2, we introduce the numerical model and procedures used to prepare and simulate spherical agglomerates. In Section 3, we discuss the evolution of the granule strength as a function of axial strain and the effects of particle size span and liquid volume. In Section 4, we introduce an analytical model of granule strength in terms of texture parameters. We conclude in Section 5 with a short summary of salient results and routes to further research.

2. Numerical method and procedures

The Discrete Element Method (DEM) has been extensively used for the simulation of granular materials [42–45]. It is based on the step-wise integration of the equations of motion for all particles by taking into account the particle interactions. In advanced applications of the DEM, it is now possible to implement also the presence of an interstitial fluid or a solid binding matrix [11,46]. However, such applications require substantially more computation power and memory in order to discretize the degrees of freedom associated with the interstitial phase. For this reason, in DEM simulations of granular processes, it is necessary to set up a modeling strategy by making appropriate choices that allow for a balance between computational efficiency (large number of particles) and physical realism. In the case of unsaturated wet granular materials, it is found that the fluid phase can be correctly represented by its cohesive and viscous effect in the particle-particle interactions [47]. Hence, we rely on this approach to model the binding liquid in the granulation process.

On the other hand, the granule strength depends on its internal structure, which is controlled to some extent by the granulation device. Here, we are interested in the simpler case of 'ideal' granules of spherical shape where the primary particles and binding liquid are homogeneously distributed. This simplification allows us to investigate the effect of basic parameters such as the particle size distribution and friction between particles on the strength in the absence of specific granulation process parameters. Furthermore, in association with texture analysis, the results of this investigation can provide a reference behavior against which the effects of process parameters can be quantified in the next step. We use the DEM with a capillary force law and a simple algorithm for the construction of spherical granules. It is worth mentioning here

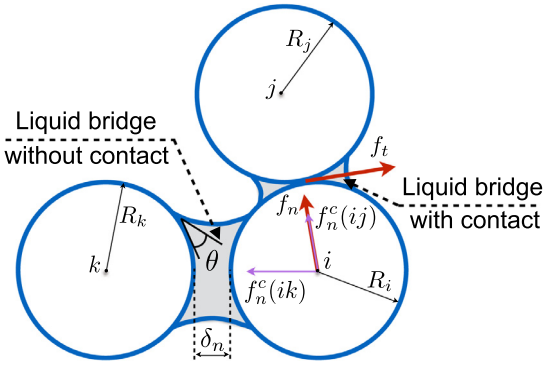

Fig. 1. Schematic drawing of the forces acting on particle i by a contacting particle j and by a non-contacting neighboring particle k.

that this approach has been used for the simulation of an assembly of wet agglomerates in the pendular state in application to powder processes such as the coalescence of granules upon collision [48] and impact breakage of crystalline agglomerates [49–52]. In this section, we describe both the numerical method and the procedure that we used to create our 'ideal' granules.

2.1. Numerical method

In the DEM, the particles are modeled as rigid particles interacting via visco-elastic force laws relating the contact force to the local strain expressed from the relative particle displacements. The simulation of rigid particles requires a stiff repulsive potential and high time resolution. The motion of each particle i with radius R_i is governed by Newton's second law:

$$m_i \frac{d^2\mathbf{s}_i}{dt^2} = f_n\mathbf{n} + f_t\mathbf{t}, \tag{1}$$

where f_n and f_t are the normal and tangential components, respectively, and $\mathbf{n}$ and $\mathbf{t}$ are the corresponding unit vectors pointing in the normal and tangential directions. m_i and $\mathbf{s}_i$ are the mass and position vector of particle i, respectively. In our simulations, we used the velocity-Verlet time-stepping scheme [45,53].

The force laws involve normal repulsion, normal damping, capillary cohesion and Coulomb friction. The normal force f_n has three different sources:

$$f_n = f_n^e + f_n^d + f_n^c. \tag{2}$$

The first term in this equation is the normal repulsive contact force. The normal repulsion force is a linear function of the normal elastic deflection δ_n approximated by the overlap between two particles [54,55]:

$$f_n^e = k_n\delta_n, \tag{3}$$

where k_n is the normal stiffness constant. The normal damping force f_n^d is assumed to be a viscous force proportional to the relative normal velocity $\dot{\delta}_n$: $f_n^d = \gamma_n\dot{\delta}_n$, where γ_n is the damping coefficient. Both these forces disappear when there is no overlap, i.e. for $\delta_n > 0$.

The last term in the Eq. (2) is the capillary cohesion force f_n^c due to the liquid bond between two particles. It depends on the gap, which we denote by δ_n as for overlaps but with negative values (positive values representing a contact deflection), liquid volume V_b, surface tension γ_s, and the particle-liquid-gas contact angle θ; see Fig. 1 [11,47,54]. The capillary cohesion force can be determined by integrating the Laplace-Young equations. Various solutions have been proposed for this equation including recent new analytical solutions [56,57]. We use the following explicit

expression of the capillary force, which is in good agreement with experiments [28,58]:

$$f_n^c = \begin{cases} -\kappa\ R, & \text{for } \delta_n < 0, \\ -\kappa\ R\ e^{-\delta_n/\lambda}, & \text{for } 0 \le \delta_n \le d_{rupt}, \\ 0, & \text{for } \delta_n > d_{rupt}, \end{cases} \tag{4}$$

where $R = \sqrt{R_i R_j}$ is the geometrical mean of the particle radii R_i and R_j, and [58]

$$\kappa = 2\pi\gamma_s \cos\theta \tag{5}$$

where d_{rupt} is the debonding distance, defined as the distance beyond which the capillary bridge is unstable and the bond breaks. It is related to liquid volume by [54,55]:

$$d_{rupt} = \left(1 + \frac{\theta}{2}\right) V_b^{1/3} \tag{6}$$

The length λ is the factor that controls the exponential falloff of the capillary attraction force in Eq. (4). This factor is a function of liquid volume V_b, the harmonic mean radius ($R' = 2R_iR_j/(R_i + R_j)$) and the size ratio between two particles in contact $r = \max\{R_i/R_j; R_j/R_i\}$:

$$\lambda = c\ h(r)\ \left(\frac{V_b}{R'}\right)^{1/2} \tag{7}$$

This form fits well the capillary force obtained from direct integration of the Laplace-Young equation by setting $h(r) = r^{-1/2}$ and $c \simeq 0.9$ [54,58,59]. The capillary force declines in absolute value as a function of the gap δ_n up to the debonding distance d_{rupt}.

For the tangential force f_t between particles in contact, we use a combination of a tangential elastic force $k_t\delta_t$, where k_t is the tangential stiffness constant, a Coulomb friction force threshold $\mu(f_n - f_n^c)$, where μ is the friction coefficient, and a tangential damping term $\gamma_t\dot{\delta}_t$, where γ_t is the tangential damping parameter and $\dot{\delta}_t$ is the contact tangential velocity [58,60–62]:

$$f_t = -\min\left\{(k_t\delta_t + \gamma_t\dot{\delta}_t), \mu(f_n - f_n^c)\right\}. \tag{8}$$

2.2. Ideal granules

In order to create homogeneous agglomerates of particles of spherical shape, we first prepared large samples by means of isotropic compaction inside a box. The primary particles are spheres with their diameters defined in a range $[d_{\min}, d_{\max}]$ with a given size ratio $\alpha = d_{\max}/d_{\min}$. The size distribution is assumed to be uniform by particle volume fractions, i.e. with all size classes having the same volume. As the total volume of particles in each size class d_i is proportional to d_i^3, the uniform distribution by volume fractions is defined by the condition that the product $n_i d_i^3$ is a constant and $\Sigma_i P_i = 1$, where P_i is the numerical fraction of particles in class i. These conditions lead to the following distribution P of particles of diameters d:

$$P(d) = 2\frac{d_{max}^2 d_{min}^2}{d_{max}^2 - d_{min}^2} d^{-3} \tag{9}$$

This distribution has the advantage of allowing the particles belonging to each size class to be correctly represented by their volume, i.e. a large number of small particles and a small number of large particles. This distribution leads to a dense packing as the pore space between large particles is filled by smaller particles [63,64].

We constructed different samples with five different values of the size ratio α= 1, 2, 3, 4 and 5. Note that the mean particle diameter $\langle d\rangle$ is a function of $d_{\min}$ and $d_{\max}$:

$$\langle d\rangle = \int_{d_{min}}^{d_{max}} d\ P(d)\delta d = d_{min}\frac{2\alpha}{1+\alpha} = d_{max}\frac{2}{1+\alpha} \tag{10}$$

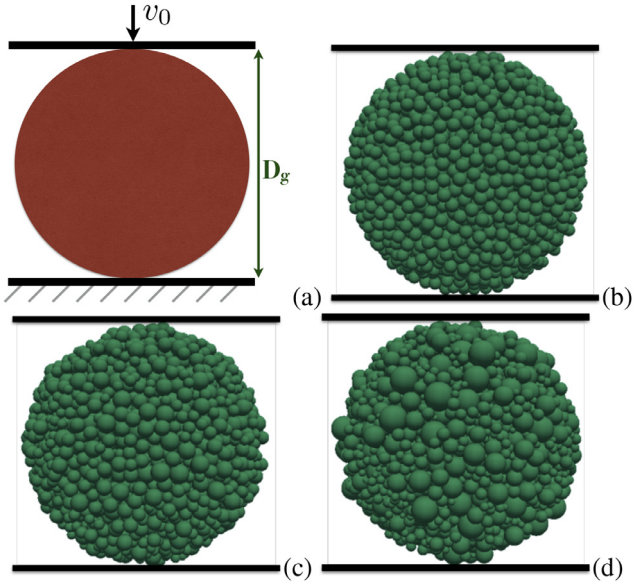

Fig. 2. Schematic representation of diametrical compression test (a), and snapshots of granules composed from 5000 primary spherical particles before diametrical compression for (b) $\alpha = 1$; (c) $\alpha = 2$, and (d) $\alpha = 5$.

The largest particle size was kept to a constant value $d_{\max} = 10$ µm, and $d_{\min}$ was decreased from 10 µm to 2 µm. Eq. (10) shows that, since $d_{\max}$ is fixed, the average diameter $\langle d\rangle$ declines by a factor 3 when α is increased from 1 to 5.

For isotropic compaction, the particles were introduced in a box and equal compressive stresses σ_0 were applied to the box walls without gravity until a packing in static equilibrium was achieved. During this step, the capillary force was set to zero and the friction coefficient to 0.1 at all contacts between particles in order to obtain a dense sample. Once all particles reached a state of static equilibrium, a spherical probe was placed in the center of the box and its radius was increased until exactly 5000 particles were inside the probe. These particles were then extracted and allowed to relax with the capillary force law activated. The common numerical parameters in these simulations are $\theta = 0$, $\gamma_n = \gamma_t = 5 \times 10^{-5}$ Ns/m and $\gamma_s = 0.072$ N/m (water).

We subjected the granules prepared by the above procedure to axial compression between two platens, as illustrated in Fig. 2(a). The bottom platen is fixed and a downward motion is applied to the top platen with a constant velocity $v_0 = 0.1$ ms^{-}1. Hence, with time step $\delta t = 10^{-9}$s used in our simulations, the total downward displacement during one time step is $v_0\delta t = 10^{-10}$ m, which is 10^{-5} times the size of the primary particles. This means that the diametrical deformation applied to the granules is slow enough to allow for a quasi-static compression test.

To see how quasi-static is the compression, one may also compare the average elastic force increment δf_e between particles with the cohesive force $f_c = \pi\gamma_s d$. The incremental force between particles is simply given by the contact normal stiffness k_n multiplied by the average normal displacement δ_n at the contact points between primary particles. The latter is given by the mean diametral deformation $v_0\delta t/D_g$ times the primary particle size d. We thus can define the dimensionless index:

$$I_e = \frac{\delta f_e}{f_c} = \frac{k_n\delta t}{\pi\gamma_s}\frac{v_0}{D_g}. \tag{11}$$

For monodisperse particles, from our parameter values we get $I_e \simeq 2.5 \times 10^{-3}$, which means that the force increments are generally small compared to the cohesion force. Finally, the time associated with the dissipation of kinetic energy is given by the ra-

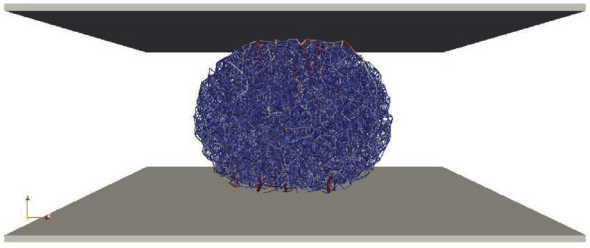

Fig. 3. Snapshot of a granule under diametrical compression for $\alpha = 1$. The lines are force chains joining the particle centers.

tio $\langle m\rangle/\gamma_n \simeq 10^{-6}$ s, which is small compared to the loading rate defined by $\langle d\rangle/v_0 \simeq 10^{-4}$ s, showing that the dissipation of the kinetic energy occurs much faster than the typical time evolution of the aggregate.

Figs. 2(b), (c) and (d) show the initial states of the granules with three different values of α before diametrical compression. In Fig. 3, we display a snapshot of a granule for $\alpha = 1$ at the end of diametrical compression. At the beginning of the test, at most three primary particles of the granule are in contact with either of the two platens. As the compression proceeds, the granule spreads without breaking between the two platens and the number of contacts between the granule and each platen increases.

The mechanical response of the granule under diametrical compression requires a measure of the axial force and vertical deformation. The vertical deformation in compression is given by

$$\varepsilon = \ln\left(1 + \frac{\Delta h}{D_g}\right) \approx \frac{\Delta h}{D_g} \tag{12}$$

where $\Delta h = v_0 t$ is the total downward displacement of the top platen (the lower platen being fixed). We also measure the vertical force component F between the granule and the top platen by summing up the normal forces between the primary particles and the platen. Let us note that, as the granule is in static equilibrium, all forces at each horizontal layer of the granule are balanced so that the vertical force acting between all horizontal layers is equal to F. By dividing this force by the sectional area πa^2 of the granule, where a is the radius of the central section of the granule perpendicular to the compression axis, we get the average vertical stress $\sigma'_{zz} = F/(\pi a^2)$ in the center of the granule. The value of a is estimated from the positions of the particles located at the boundary of the actual central section.

The stress can also be obtained from the values of normal forces and branch vectors (vectors joining particle centers) using [65–69]

$$\sigma_{zz} = \frac{1}{V_g}\sum_{k=1}^{N_b} f_z^k \ell_z^k = n_b \langle f_z^k \ell_z^k\rangle_k, \tag{13}$$

where V_g is the volume of the granule, N_b is the number of bonds, $n_b = N_b/V_g$ is the number density of bonds, f_z^k and ℓ_z^k are the z-components of the bond force vector and branch vector, respectively, at the contact k, including all internal contacts as well as the contacts with the platens. The symbol $\langle\cdots\rangle_k$ denotes averaging over all contacts k in the volume. We find that $\sigma_{zz} \simeq \sigma'_{zz}$ during vertical compression. Note that we can define a characteristic cohesive stress σ_c from the capillary force and the mean particle diameter $\langle d\rangle$:

$$\sigma_c = \frac{\kappa}{\langle d\rangle} \tag{14}$$

This stress depends on $\langle d\rangle$ and, by virtue of Eq. (10), varies linearly with α as

$$\sigma_c = \frac{\kappa}{d_{max}}\frac{1+\alpha}{2} \tag{15}$$

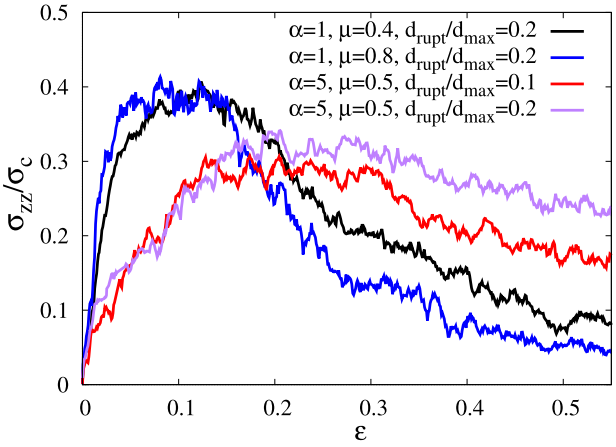

Fig. 4. Vertical strength σ_{zz} normalized by the reference stress σ_c for different values of friction coefficient μ, size ratio α and the debonding distance d_{rupt}, as a function of cumulative vertical strain ε.

Its value increases in our simulations by a factor 3 as α is increased from 1 to 5 by reducing $d_{\min}$.

3. Granule strength

Fig. 4 shows the evolution of the mean vertical stress σ_{zz} normalized by the reference cohesive stress σ_c as a function of the vertical strain ε for different values of granule parameters. In all cases, σ_{zz} first increases with strain and reaches a plateau more or less fast depending on the values of parameters. It then declines smoothly as a result of the gradual loss of cohesive contacts. The stress plateau is a signature of plastic deformation due to particle rearrangements. However, this plateau does not persist as the cohesive contacts break apart and do not heal. This irreversible character of cohesive contacts is assumed to reflect the fact that the liquid contained in a capillary bridge between two particles is not physically available (e.g. due to evaporation or drainage) once the bridge disappears. This may not always be the case as liquid drops may survive at the surface of the particles and migrate through the vapor phase or by diffusion at the surface of the particles to the newly-formed contacts during a continuous deformation of the granule.

In this way, the observed behavior can globally be qualified as ductile with a well-defined plastic plateau before the beginning of a progressive loss of cohesion at strains above 0.2. This means that the debonding events between primary particles do not lead to spontaneous formation of a fracture surface. We also see that the plastic stress threshold σ_p is of the order of $0.4\sigma_c$ for monodisperse particles and $0.3\sigma_c$ for $\alpha = 5$. On the plateau, the particles are well-connected with one another, and the loss of one or two cohesive bonds of a particle does not lead to macroscopic rupture. The values of parameters affect not only the plastic threshold but also the initial build-up and later fall-off of the stress.

The effect of size span α on the plastic strength is displayed in Fig. 5 for several values of the debonding distance d_{rupt}. We see that the ratio σ_p/σ_c declines by nearly the same amount in all cases as α increases from 1 to 5. This is, however, only a small relative loss of strength with respect to σ_c given that, according to Eq. (15), σ_c is multiplied by 3 when α increases from 1 to 5. Hence, in absolute value, the cohesive strength of the granule increases by nearly a factor 3 as shown in the inset to Fig. 5. Fig. 6 displays the cohesive (plastic) strength as a function of d_{rupt} for different values of α. We see that this dependence is linear and quite weak for all values of α. As we shall see in the next section, this increase of cohesive strength reflects that of the connectivity

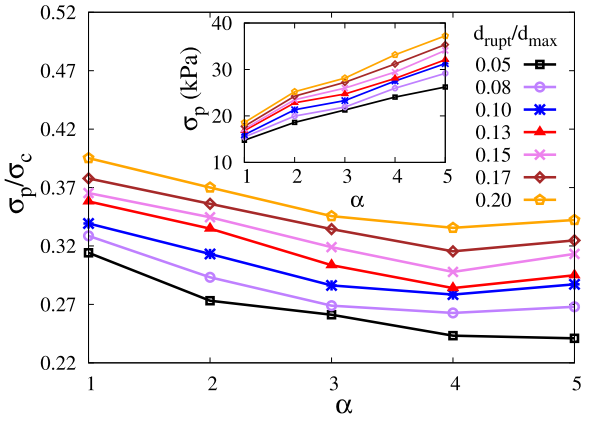

Fig. 5. Normalized plastic strength of the granule for several values of the debonding distance as a function of the size ratio α. The inset shows the non-normalized value of the strength as a function of α.

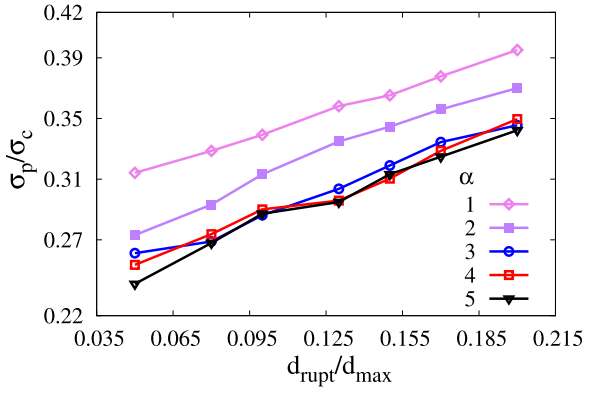

Fig. 6. Normalized plastic strength σ_p/σ_c of the granules for different values of the size ratio as function of debonding distance d_{rupt}.

of primary particles by liquid bonds as the debonding distance increases.

4. Analytical model

The granule strength under diametrical compression reflects the microstructure of the granule, which depends in our simulations on the effects of size span and debonding distance (related to the amount of liquid). The granular microstructure can be described in terms of various scalar and tensorial variables such as the coordination number, packing fraction and fabric tensor [70]. Fig. 7 shows that the initial value of the wet coordination number Z_0 is an increasing function of both α and the debonding distance d_{rupt}. The wet coordination number is defined as the number of capillary bonds per particle. This is slightly above the "dry" coordination number, which accounts for only the geometrically touching particles. We see that the increase of Z_0 is more significant with d_{rupt} than with α. Its increase is nonlinear with d_{rupt} and it levels off around $Z_0 = 12$.

In order to get a more clear understanding of the relation between the connectivity of particles and the plastic strength, we may use the expression (13) of the stress tensor applied in our case to the whole volume V_g of the granule. To obtain an analytical expression of the cohesive stress, we consider the cohesive forces $f_c^{ij} = \pi\gamma_s\sqrt{d_i d_j}$ between particles of diameters d_i and d_j. Most of the cohesive strength is carried by this cohesive force acting between particles that are in contact. But many particles are connected by capillary bridges with a nonzero gap, where the cohesive force is below f_c^{ij} [59]. At plastic threshold, a large number of

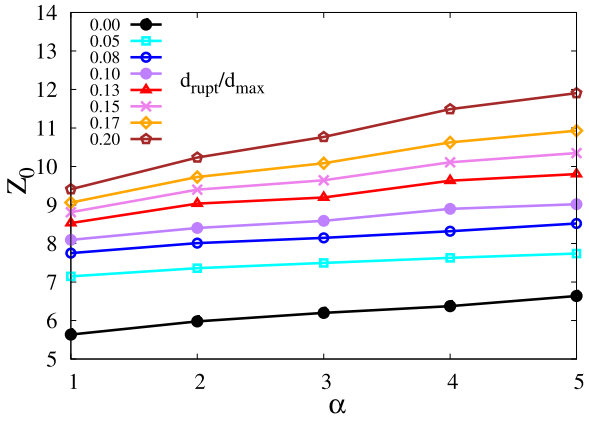

Fig. 7. The initial wet coordination number Z_0 of the granules for different values of debonding distance as a function of the size ratio α.

bonds along the directions perpendicular to the compression axis are tensile whereas many others along the compression axis are compressive.

The ductility of the particle at failure is induced by the effect of tensile bonds that prevent the primary particles from sudden rupture. We will account below for these bonds by a prefactor estimated from simulations. The vertical component at plastic threshold is given by

$$\sigma_p = \sigma_{zz} = n_b\langle f_c^{(ij)}\ell^{(ij)}\rangle_{(ij)}\langle\cos^2\theta_z^{(ij)}\rangle_{(ij)}, \tag{16}$$

where the summation runs over all contacts (ij) and we have

$$\ell^{ij} = \frac{1}{2}(d_i + d_j) \tag{17}$$

The angle $\theta_z^{(ij)}$ is the angle between the contact normal and the vertical axis. This angle is assumed to be uncorrelated with $f_c^{(ij)}\ell^{(ij)}$. For a nearly isotropic distribution of contact orientations, we have $\langle\cos^2\theta_z\rangle = 1/3$, so that

$$\sigma_p = \frac{\kappa}{12}n_b\langle(d_i + d_j)\sqrt{d_i d_j}\rangle_{(ij)} \tag{18}$$

The number density (number per unit volume) n_b of bonds can be estimated as the number of bonds per particle $Z/2$ divided by the free volume V_f occupied by each particle. This volume is simply the particle volume divided by the mean packing fraction Φ of the granule such that the sum of all particle free volumes is equal to the granule volume V_g. Hence,

$$V_f = \frac{\pi}{6\Phi}\langle d^3\rangle \tag{19}$$

so that

$$n_b = \frac{Z}{2V_f} = \frac{3Z\Phi}{\pi\langle d^3\rangle} \tag{20}$$

Introducing this expression in Eq. (18), we get

$$\sigma_p = \frac{Z\Phi\kappa}{4\pi}\frac{\langle(d_i + d_j)\sqrt{d_i d_j}\rangle}{\langle d^3\rangle} \tag{21}$$

The geometric factor $\langle(d_i + d_j)\sqrt{d_i d_j}\rangle$ can be evaluated as [54]

$$\begin{aligned}\langle(d_i + d_j)\sqrt{d_i d_j}\rangle &= \langle d_i^{3/2}d_j^{1/2}\rangle + \langle d_j^{3/2}d_i^{1/2}\rangle \\ &= 2\langle d^{3/2}\rangle\langle d^{1/2}\rangle\end{aligned} \tag{22}$$

with the underlying assumption that there is no size segregation so that d_i and d_j are not correlated. Hence, we finally get

$$\sigma_p = \eta\frac{sZ\Phi}{2\pi}\frac{\kappa}{\langle d\rangle} = \eta\frac{sZ\Phi}{2\pi}\sigma_c \tag{23}$$

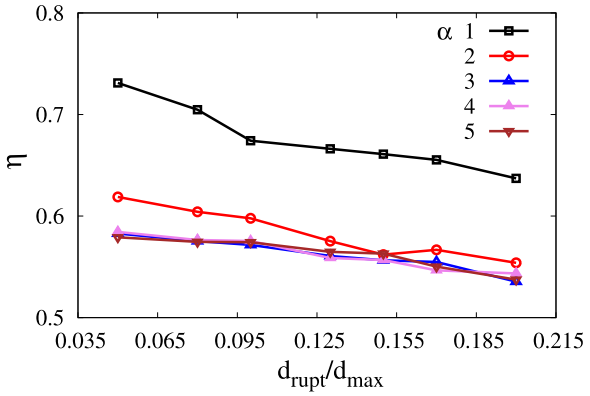

Fig. 8. The prefactor η in Eq. (23) as a function of the debonding distance d_{rupt} for different values of α.

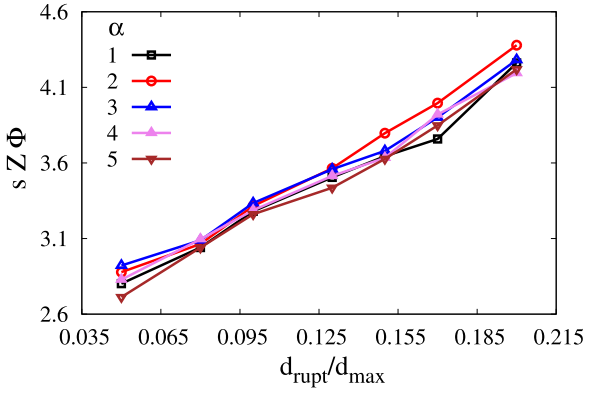

Fig. 9. The $Z\Phi s$ in Eq. (23) as a function of the debonding distance d_{rupt} for different values of α.

with

$$s = \frac{\langle d^{1/2}\rangle \langle d\rangle \langle d^{3/2}\rangle}{\langle d^3\rangle} \tag{24}$$

The prefactor η is introduced here to account for the bonds with a nonzero gap where the cohesive force is below f_c^{ij}. Since Z denotes the coordination number for capillary bonds, Eq. (23) with $\eta = 1$ can be considered as an upper bound for the plastic strength. In the same way, for Z equal to the coordination number only for contacts, Eq. (23) provides a lower bound of the plastic strength. As Z varies between 8 and 12 (see Fig. 7), we thus expect that η is generally below but close to 1.

Fig. 8 displays the values of η computed from our simulations for all values of α and d_{rupt}. We see that η declines slightly with α and d_{rupt}. For small values of d_{rupt}, its value is $\simeq 0.7$ for monodisperse granules and $\simeq 0.6$ for polydisperse granules. With this prefactor, Eq. (23) predicts that the dependence of the normalized strength σ_p/σ_c with respect to α and d_{rupt} is mediated by that of $sZ\Phi$. Fig. 9 displays $sZ\Phi$ as a function of $d_{rupt}/d_{\max}$ for different values of α. Interestingly, up to insignificant statistical fluctuations, $sZ\Phi$ is independent of α and a nearly linear function of $d_{rupt}/d_{\max}$ as that of σ_p in Fig. 6.

We see that the analytical model presented in this section correctly links the microstructure to the overall strength of the agglomerate. The trends are well predicted by the model up to the prefactor η, which appears to be weakly dependent on the material parameters. The physical interpretation of its value may be related to the presence of the large proportion of capillary bonds with nonzero gap, as briefly discussed previously. However, it may also be a consequence of the inhomogeneous stress transmission inside the agglomerate.

5. Conclusions

In this paper, we used a 3D particle dynamics algorithm together with a capillary force law to analyze the cohesive strength and microstructure of spherical agglomerates. The agglomerates were constructed by extraction of spherical samples from a granular bed prepared by compaction for different values of particle size span, and subjected to diametrical compression between two platens for different values of debonding distance, which accounts for the amount of liquid in the capillary bonds. Despite the irreversible nature of cohesive bonds (i.e. no new cohesive bond), we observe a plastic plateau before the onset of failure. We showed that the plastic strength is proportional to the characteristic capillary stress $\gamma_s/\langle d\rangle$ with a multiplicative factor that is a linear function of the debonding distance, increases with the size ratio and is nearly independent of the friction coefficient (not shown here). We also introduced an analytical expression of the cohesive strength in terms of the packing fraction, wet coordination number, size polydispersity and debonding distance. This model is in excellent agreement with the observed trends up to a prefactor that we estimated from the numerical data, and which is weakly dependent on the material parameters.

As previously discussed in this paper, our results provide the behavior of an 'ideal' granule in the sense that the granules were not created by an agglomeration process. We presently work on the simulation of the granulation process in a rotating drum that will allow us to investigate the important complementary problem of predicting the agglomerate microstructure from the process parameters such as rotating speed and filling rate. The ideal granule can then be used as a reference system with which we will compare part of our results. Given the broad applications of the agglomeration process, it is also desirable to validate the simulations by comparison with experimental observations. Systematic diametrical compression tests are presently underway in order to determine the effects of material parameters on the granule strength allowing for the validation of numerical results. Our experiments are in good agreement with the order of magnitude of the cohesive strength of agglomerates for $\eta \simeq 0.4$. In these experiments, particles of the same typical size as in simulations were used. They were mixed with water and agglomerated into granules in a rotating drum. Preliminary experimental results were presented in [71].

References

[1] S.M. Iveson, J.D. Litster, K. Hapgood, B.J. Ennis, Nucleation, growth and breakage phenomena in agitated wet granulation processes: a review, Powder Technol. 117 (1) (2001) 3–39.
[2] S. Herminghaus, Dynamics of wet granular matter, Adv. Phys. 54 (3) (2005) 221–261.
[3] J. Litster, B. Ennis, The science and engineering of granulation processes, 15, Springer, Netherlands, 2014.
[4] C. Liao, S. Hsiau, S. Wen, Effect of adding a small amount of liquid on density-induced wet granular segregation in a rotating drum, Adv. Powder Technol. 27 (4) (2016) 1265–1271.
[5] J. Degrève, J. Baeyens, M.V. de Velden, S.D. Laet, Spray-agglomeration of npk-fertilizer in a rotating drum granulator, Powder Technol. 163 (3) (2006) 188–195.
[6] J.D. Osborne, R.P. Sochon, J.J. Cartwright, D.G. Doughty, M.J. Hounslow, A.D. Salman, Binder addition methods and binder distribution in high shear and fluidised bed granulation, Chem. Eng. Res. Des. 89 (5) (2011) 553–559.
[7] S.K. Pawar, F. Henrikson, G. Finotello, J.T. Padding, N.G. Deen, A. Jongsma, F. Innings, J.H. Kuipers, An experimental study of droplet-particle collisions, Powder Technol. 300 (2016) 157–163.
[8] R. Pashminehazar, A. Kharaghani, E. Tsotsas, Three dimensional characterization of morphology and internal structure of soft material agglomerates produced in spray fluidized bed by X-ray tomography, Powder Technol. 300 (2016) 46–60.
[9] S. Iveson, J. Litster, Growth regime map for liquid-bound granules, AlChE J. 44 (7) (1998) 1510–1518.
[10] Delenne, J. Y., Richefeu, V., & Radjai, F.. Liquid clustering and capillary pressure in granular media. J. Fluid Mech., 762.

[11] G. Lian, C. Thornton, M. Adams, A theoretical study of the liquid bridge forces between two rigid spherical bodies, J. Colloid Interface Sci. 161 (1993) 138–147.
[12] C. Willett, M. Adans, S. Johnson, J. Seville, Capillary bridges between two spherical bodies, Langmuir 16 (2000) 9396–9405.
[13] F. Štěpánek, P. Rajniak, C. Mancinelli, R. Chern, R. Ramachandran, Distribution and accessibility of binder in wet granules, Powder Technol. 189 (2) (2009) 376–384.
[14] M. Scheel, R. Seemann, M. Brinkmann, M.D. Michiel, A. Sheppard, S. Herminghaus, Liquid distribution and cohesion in wet granular assemblies beyond the capillary bridge regime, J. Phys. Condens. Matter 20 (49) (2008) 236–494.
[15] S. Iveson, J. Beathe, N. Page, The dynamic strength of partially saturated powder compacts: the effect of liquid properties, Powder Technol. 127 (2002) 149–161.
[16] C. Thornton, Z. Ning, A theoretical model for the stick/bounce behaviour of adhesive, elastic-plastic spheres, Powder Technol. 99 (2) (1998) 154–162.
[17] L.X. Liu, J.D. Litster, S.M. Iveson, B.J. Ennis, Coalescence of deformable granules in wet granulation processes, AlChE J. 46 (2000) 529–539.
[18] M. Ghadiri, A.D. Salman, M. Hounslow, A. Hassanpour, D.W. York, Editorial: special issue – agglomeration, Chem. Eng. Res. Des. 89 (5) (2011) 499.
[19] J. Rojek, S. Nosewicz, M. Maździarz, P. Kowalczyk, K. Wawrzyk, D. Lumelskyj, Modeling of a sintering process at various scales, Procedia Eng. 177 (2017) 263–270.
[20] N. Rahmanian, A. Naji, M. Ghadiri, Effects of process parameters on granules properties produced in a high shear granulator, Chem. Eng. Res. Des. 89 (5) (2011) 512–518.
[21] K.E. Ileleji, Y. Li, R.K. Ambrose, P.H. Doane, Experimental investigations towards understanding important parameters in wet drum granulation of corn stover biomass, Powder Technol. 300 (2016) 126–135.
[22] R. Ramachandran, J.M.H. Poon, C.F. Sanders, T. Glaser, C.D. Immanuel, F.J. Doyle, J.D. Litster, F. Stepanek, F.Y. Wang, I.T. Cameron, Experimental studies on distributions of granule size, binder content and porosity in batch drum granulation: inferences on process modelling requirements and process sensitivities, Powder Technol. 188 (2) (2008) 89–101.
[23] S. Iveson, J. Litster, B. Ennis, Fundamental studies of granule consolidation part 1: effects of binder content and binder viscosity, Powder Technol. 88 (1) (1996) 15–20.
[24] S.M. Iveson, P.A. Wauters, S. Forrest, J.D. Litster, G.M. Meesters, B. Scarlett, Growth regime map for liquid-bound granules: further development and experimental validation, Powder Technol. 117 (1–2) (2001) 83–97.
[25] B. Mishra, C. Thornton, D. Bhimji, A preliminary numerical investigation of agglomeration in a rotary drum, Miner. Eng. 15 (1) (2002) 27–33.
[26] P.A. Wauters, R.B. Jakobsen, J.D. Litster, G.M. Meesters, B. Scarlett, Liquid distribution as a means to describing the granule growth mechanism, Powder Technol. 123 (2) (2002) 166–177.
[27] F. Štěpánek, M. Ansari, Computer simulation of granule microstructure formation, Chem. Eng. Sci 60 (14) (2005) 4019–4029.
[28] T. Mikami, H. Kamiya, M. Horio, Numerical simulation of cohesive powder behavior in a fluidized bed, Chem. Eng. Sci. 53 (10) (1998) 1927–1940.
[29] R. Aguado, S. Roudier, L. Delagado, Best Available Techniques (BAT) Reference Document for Iron and Steel Production., Joint research centre of the european commission, luxembourg: Publications office of the european union, 2013.
[30] G. Lefebvre, P. Jop, Erosion dynamics of a wet granular medium, Physic. Rev. E Stat. Nonlin.Soft Matt. Phy. 8 (2013) 032–205.
[31] K.V. Sastry, P. Dontula, C. Hosten, Investigation of the layering mechanism of agglomerate growth during drum pelletization, Powder Technol. 130 (1) (2003) 231–237.
[32] P. Wauters, R. van de Water, J. Litster, G. Meesters, B. Scarlett, Growth and compaction behaviour of copper concentrate granules in a rotating drum, Powder Technol. 124 (3) (2002) 230–237.
[33] I. Govender, Granular flows in rotating drums: a rheological perspective, Miner. Eng. 92 (2016) 168–175.
[34] Berger, N., Azéma, E., Douce, J. F., & Radjai, F.. Scaling behaviour of cohesive granular flows. EPL-Europhys. Lett., 112.
[35] B. Song, S. Rough, D. Wilson, Effects of drying technique on extrusion–spheronisation granules and tablet properties, Int. J. Pharm. 332 (1) (2007) 38–44.
[36] F. Fichtner, A. Rasmuson, G. Alderborn, Particle size distribution and evolution in tablet structure during and after compaction, Int. J. Pharm. 292 (1) (2005) 211–225.
[37] C.Y. Wu, S.M. Best, A.C. Bentham, B.C. Hancock, W. Bonfield, A simple predictive model for the tensile strength of binary tablets, Eur. J. Pharm. Sci. 25 (2) (2005) 331–336.
[38] O. Tsoungui, D. Vallet, J.C. Charmet, Numerical model of crushing of grains inside two-dimensional granular materials, Powder Technol. 105 (1) (1999) 190–198.
[39] J. Fu, G.K. Reynolds, M.J. Adams, M.J. Hounslow, A.D. Salman, An experimental study of the impact breakage of wet granules, Chem. Eng. Sci. 60 (14) (2005) 4005–4018.
[40] D.H. Nguyen, E. Azéma, P. Sornay, F. Radjai, Bonded-cell model for particle fracture, Phys. Rev. E. 91 (2015) 022–203.
[41] D. Cantor, E. Azéma, P. Sornay, F. Radjai, Three-dimensional bonded-cell model for grain fragmentation, Comput. Part. Mech. (2016) 1–10.
[42] P.A. Cundall, O.D.L. Strack, A discrete numerical model for granular assemblies, Géotechnique 29 (1) (1979) 47–65.
[43] C. Thornton, Quasi-static shear deformation of a soft particle system, Powder Technol. 109 (1999) 179–191.
[44] H.J. Herrmann, S. Luding, Modeling granular media with the computer, Continuum Mech. Thermodyn. 10 (1998) 189–231.
[45] F. Radjai, F. Dubois, Discrete-element Modeling of Granular Materials, Wiley-iste, 2011.
[46] F. Radjai, V. Topin, V. Richefeu, C. Voivret, J.Y. Delenne, E. Azéma, M.S.E. Youssoufi, Force Transmission in Cohesive Granular Media, in: J.D. Goddard, J.T. Jenkins, P. Giovine (Eds.), Mathematical modeling and physical instances of granular flows, AIP, 2010, pp. 240–260.
[47] V. Richefeu, M.S.E. Youssoufi, F. Radjaï, Shear Strength of Unsaturated Soils: Experiments, Dem Simulations, and Micromechanical Analysis, in: Theoretical and numerical unsaturated soil mechanics, springer, 2007, pp. 83–91.
[48] G. Lian, C. Thornton, M.J. Adams, Discrete particle simulation of agglomerate impact coalescence, Chem. Eng. Sci. 53 (19) (1998) 3381–3391.
[49] K. Kafui, C. Thornton, Numerical simulations of impact breakage of a spherical crystalline agglomerate, Powder Technol. 109 (1) (2000) 113–132.
[50] B. Mishra, C. Thornton, Impact breakage of particle agglomerates, Int. J. Miner. Process. 61 (4) (2001) 225–239.
[51] C. Thornton, M.T. Ciomocos, M.J. Adams, Numerical simulations of diametrical compression tests on agglomerates, Powder Technol. 140 (2004) 258–267.
[52] L. Liu, K. Kafui, C. Thornton, Impact breakage of spherical, cuboidal and cylindrical agglomerates, Powder Technol. 199 (2) (2010) 189–196.
[53] J. Duran, A. Reisinger, P. de Gennes, Sands, Powders, and Grains: An Introduction to the Physics of Granular Materials, Partially ordered systems, Springer, New York, 1999.
[54] V. Richefeu, M.E. Youssoufi, F. Radjai, F., Shear strength properties of wet granular materials, Physic. Rev. E. 73 (2006) 051–304.
[55] T.-T. Vo, P. Mutabaruka, J.-Y. Delenne, S. Nezamabadi, F. Radjai, Strength of wet agglomerates of spherical particles: effects of friction and size distribution, EPJ Web Conf. 140 (2017) 08021.
[56] G. Gagneux, O. Millet, Analytic calculation of capillary bridge properties deduced as an inverse problem from experimental data, Transp. Porous Media 105 (2014) 117–139.
[57] G. Lian, J. Seville, The capillary bridge between two spheres: new closed-form equations in a two century old problem, Adv. Colloid Interface Sci. 227 (2016) 53–62.
[58] V. Richefeu, F. Radjai, M.S.E. Youssoufi, Stress transmission in wet granular materials., Eur. Phys. J. E. 21 (2007) 359–369.
[59] F. Radjaï, V. Richefeu, Bond anisotropy and cohesion of wet granular materials, Philosophic. Trans. Royal Soc. A 367 (2009) 5123–5138.
[60] J. Schäfer, S. Dippel, D.E. Wolf, Force schemes in simulations of granular materials, J. Phys. I. France 6 (1996) 5–20.
[61] S. Dippel, G.G. Batrouni, D.E. Wolf, How transversal fluctuations affect the friction of a particle on a rough incline, Phys. Rev. E. 56 (1997) 3645–3656.
[62] S. Luding, Collisions and Contacts between Two Particles, in: H.J. Herrmann, J.P. Hovi, S. Luding (Eds.), Physics of dry granular media - NATO ASI series e350, Kluwer Academic Publishers, Dordrecht, 1998, p. 285.
[63] C. Voivret, F. Radjaï, J.Y. Delenne, M.S.E. Youssoufi, Space-filling properties of polydisperse granular media., Phys. Rev. E. Stat. Nonlin. Soft. Matter Phys. 76 (2 Pt 1) (2007) 01–0213.
[64] C. Voivret, F. Radjai, J.Y. Delenne, M.S.E. Youssoufi, Multiscale force networks in highly polydisperse granular media, Physic. Rev. Lett. 102 (2009) 178001.
[65] L. Rothenburg, A.P.S. Selvadurai, A Micromechanical Definition of the Cauchy Stress Tensor for Particulate Media, in: A.P.S. Selvadurai (Ed.), Mechanics of structured media, Elsevier, 1981, pp. 469–486.
[66] J. Christoffersen, M.M. Mehrabadi, S. Nemat-Nasser, A micromechanical description of granular material behavior, J. Appl. Mech. 48 (1981) 339–344.
[67] M.M. Mehrabadi, S. Nemat-Nasser, M. Oda, On statistical description of stress and fabric in granular materials, Int. J. Num. Anal. Meth. Geomech. 6 (1982) 95–108.
[68] J.J. Moreau, New Computation Methods in Granular Dynamics, in: A.A. Balkema (Ed.), Powders & grains 93, 1993, p. 227. Rotterdam
[69] L. Staron, F. Radjai, J. Vilotte, Multi-scale analysis of the stress state in a granular slope in transition to failure, Eur. Phys. J. E 18 (2005) 311–320.
[70] F. Radjai, J.N. Roux, A. Daouadji, Modeling granular materials: century-long research across scales, J. Eng. Mech. 143 (4) (2017) 0401–7002.
[71] Contreras, R. Jaimes, Berger, Nicolas, Izard, Edouard, Douce, J.-F. cois, Koltsov, Alexey, Delenne, Jean-Yves, Azema, Emilien, Nezamabadi, Saeid, van Loo, Frédéric, Pellenq, Roland, Radjai, Farhang, Cohesive strength of iron ore granules, EPJ Web Conf. 140 (2017) 08020.